J Solid State Electrochem (2009) 13:1209–1214
DOI 10.1007/s10008-008-0648-6

ORIGINAL PAPER

Improved performance of Bi_2O_3-doped MnO_2 cathode on rechargeability in LiOH aqueous cell

Manickam Minakshi

Received: 10 June 2008 / Revised: 4 August 2008 / Accepted: 6 August 2008 / Published online: 27 August 2008

Abstract Many attempts have been made to make the zinc-manganese dioxide (Zn-MnO_2) alkaline cell rechargeable, but all investigations are pertained to the proton insertion mechanism into MnO_2. In this paper, a new class of rechargeable bismuth oxide-doped MnO_2 electrode in lithium hydroxide (LiOH) electrolyte is described. The doping and the appropriate pH selection of the aqueous electrolyte improved the electrochemical performance of the aqueous cell. Hence, with an aim to understand the role of bismuth oxide (Bi_2O_3) during the discharge process, doped MnO_2 cathodes are characterized by various techniques like secondary ion mass spectrometry, X-ray diffraction, Fourier transform infra-red spectroscopy, and transmission electron microscopy analysis. The results suggest that the influence of the large radius of the cation (Bi_2O_3; Bi (III) ion (0.96 Å)) cannot be integrated into the spinel structure, thereby, improving the rechargeability. The electrode reaction of doped MnO_2 in LiOH electrolyte is shown to be lithium insertion while preventing the formation of a spinel structure that leads to a major formation of manganese oxy hydroxides.

Keywords Rechargeability · Aqueous battery · LiOH · SIMS · Bi_2O_3

M. Minakshi (✉)
Department of Extractive Metallurgy ad chemistry,
Murdoch University,
Murdoch, Western Australia 6150, Australia
e-mail: minakshi@murdoch.edu.au

Introduction

The development of inexpensive and safe cathode materials for the battery systems is currently a major focus in battery research. In this regard, manganese oxides have a long history of serving as a cathode in charged storage applications. The desirable features of manganese dioxide (MnO_2) materials are: abundantly available inexpensive transition metal, increased safety margin to overcharge conditions compared to cobalt- and nickel-based batteries [1–3]. These features made MnO_2 cathode materials more attractive for large energy storage applications like electric vehicles. Currently, MnO_2 is used in products ranging from alkaline to lithium batteries and to even super capacitors. This is because, as said above, MnO_2 is regarded as nontoxic and a common transition metal.

Rechargeable MnO_2 alkaline cells involving two electrons per manganese between Mn^{4+} and Mn^{2+} are appealing as they can provide high energy densities exceeding that of currently available lithium ion cells [4]. Additionally, with the use of aqueous electrolytes, the alkaline cells offer better safety characteristics, less expensive compared to their nonaqueous counterparts. However, the poor rechargeability of manganese dioxides in alkaline cells has hampered their use to mainly primary batteries. The formation of nonrechargeable products like $Mn(OH)_2$, Mn_2O_3, and Mn_3O_4 have been regarded as a reason for poor rechargeability [4–6].

Many efforts have been made to achieve better rechargeability with the alkaline manganese dioxide cells using potassium hydroxide as electrolyte [4–6]. In all these studies, it is commonly believed in the literature that alkaline cells are based on the proton insertion into MnO_2 [7–10] and that under certain conditions, the insertion of protons is reversible. Recently, we demonstrated that good

rechargeability could be obtained by using aqueous lithium hydroxide (LiOH) as electrolyte [11]. This involved lithium intercalation into the MnO_2 lattice.

In our previous papers [12, 13], we assessed the influence of Bi_2O_3 doped MnO_2 on the electrochemical performance of MnO_2/LiOH batteries. Although the effect of Bi_2O_3 doping into MnO_2 structure and its lithium insertion mechanism is reported by Bach et al. [14], it is investigated using nonaqueous solvents. The Bi-doped MnO_2 cathode is shown to endow an improved rechargeability regardless of the amount of Bi_2O_3 using LiOH as electrolyte [12]. However, the stability window of an aqueous electrolyte is very narrow than using nonaqueous counterparts. In the current paper, we have extended this Bi-doped study in more detail, choosing 10 wt.% of Bi_2O_3. The Bi-doped (10 wt.%) cathode showed a limited discharge capacity of 150 mAh/g in a LiOH electrolyte having a pH=12.0 [12] but not in an electrolyte having pH=10.5 in the present study. Hence, the pH selection in the aqueous electrolyte is also described here.

Experimental

The MnO_2 (IBA sample 32) material used in this work was obtained from Kerr McGee Chemical Corporation. Bismuth oxide (Bi_2O_3) was obtained from Aldrich Chemical Company. For the electrochemical test, a pellet (30 mg) of cathode mixture was prepared by mixing 65 wt.% MnO_2, 10 wt.% Bi_2O_3, 15 wt.% acetylene black (A-99, Asbury, USA) and 10 wt.% poly(vinylidene difluoride) (PVDF, Sigma Aldrich) as binder in a mortar and pestle. An electrochemical cell was constructed with the disk-like pellet (of 8 mm diameter and 0.5 mm in thickness) as the cathode, Zn metal (99.9%) as the anode, and filter paper (Whatman filters 12) as the separator. The electrolyte used was a 5-M solution of LiOH containing 1 mol L^{-1} zinc sulfate with saturated lithium carbonate present in it. The optimum pH selection for the electrolyte was 10.5. The galvanostatic discharge, charge conditions, and other experimental details were identical to those reported in [11–13].

For X-ray analysis, a Siemens X-ray diffractometer using Philips Co-Kα radiation was used. The Fourier transform infrared (FTIR) spectra were recorded by using a Nicolet Magna-IR spectrometer. For each sample, an average of 16 scans were recorded. The morphology and elemental analysis of the products formed before and after discharge were characterized by transmission electron microscopy (TEM) and energy dispersive X-ray spectroscopy (EDS) using a JEOL 2010F TEM model operated at 200 kV. TEM specimens were prepared by scraping a small fragment scraped from the pressed pellet and lightly grinding under methanol and dispersing on to a holey carbon support film. Specimens were examined at liquid nitrogen temperature in a cooling stage to reduce beam damage and contamination effects. Secondary ion mass spectra (SIMS) were collected on a Cameca ims 5f instrument at the Australian Nuclear Science and Technology Organization, Lucas Heights, Sydney, Australia. An O_2^+ primary ion source (12.5 kV) was used to generate secondary ions. A primary beam of 50 nA rastered over an area of 250× 250 μm was used in all experiments. The SIMS positive ion signals corresponding to ^7Li was recorded.

Results and discussion

1. Galvanostatic discharge–charge characteristics of Zn-(Bi_2O_3) MnO_2-LiOH cell

The galvanostatic discharge–charge profiles of the Zn-MnO_2 cells were carried out initially by discharging and then charging the cells at a constant current density of 0.5 mA/cm^2 to a cutoff voltage of 1.0 and 1.8 V, respectively. The first cycle discharge–charge voltage profiles of the Bi_2O_3-free electrodes (undoped MnO_2) and Bi_2O_3-containing (Bi_2O_3-doped MnO_2) are compared in Fig. 1. The Bi_2O_3-doped sample (Fig. 1) shows a higher discharge capacity of 215 mAh/g than the undoped MnO_2 which is 140 mAh/g. However, the differences in discharge voltage of these two materials are not significant, i.e., only 40 mV. Both the cells could be reversibly charged with the coulombic efficiencies of 91% and 86% for undoped and doped MnO_2 materials, respectively. Although the general characteristics of the discharge curves were similar for both materials, the discharge capacity for Bi_2O_3-doped (Fig. 1)

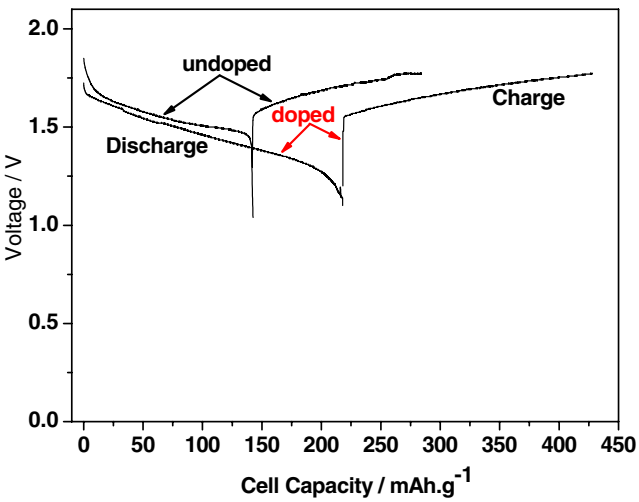

Fig. 1 The first discharge–charge behavior of undoped MnO_2 and Bi_2O_3-doped MnO_2 cathode with the pH selection of an aqueous electrolyte 10.5

was higher and a long plateau-like region is seen before undergoing a drop in potential at 1.2 V. The observed difference in the material utilization could be due to the presence of Bi_2O_3. But, on the other hand, the identical Bi_2O_3-doped sample showed a limited discharge capacity of 150 mAh/g [12]. Initially, the mechanism was unclear but then it is understood that, besides doping, the difference is also due to the stability range of electrolyte. This is the downside of employing an aqueous electrolyte in a system. While having a pH of the electrolyte=12.0, the discharge capacity is only 150 mAh/g [12]; this could be either due to dissolution of the electrode itself into the electrolyte or poor reduction process. The preferred pH value for our electrolyte in the current study of Bi-doped material is found to be 10.5, achieving a maximum discharge capacity of 215 mAh/g (in Fig. 1). This electrolyte met the conditions of high ionic conductivity and sufficient salt concentration to prevent starvation of electrolyte during the operation of the battery. Nevertheless, in both doped and undoped samples, it should be noted that the discharge capacity is also limited by the zinc anodes as the dissolved zincate ions combine with the manganese ions to give inactive zinc-manganese species and zinc precipitation on the electrode that inhibits the reduction of MnO_2 [15].

Role of Bi_2O_3 The role of Bi_2O_3 in MnO_2 is to enhance the rechargeability and lithium insertion mechanism. As the size of Bi (III) ion is sufficiently large compared to Mn (IV) and Mn (III) ions, it is a beneficial effect that Bi (III) ions prevents the formation of spinel lattice (γ-Mn_2O_3) which normally occurs in the aqueous solutions [16, 17]. The spinel lattice is well known to be a poor electroactive compound. Hence, the presence of large Bi (III) ions in the interlayer spacing of MnO_2 compound prevents the major structural changes (as shown in the X-ray diffraction (XRD) pattern in Fig. 3) and promotes the rechargeability.

Figure 2 shows the cyclability data of undoped and doped MnO_2 cathodes. The data demonstrates that good cycling performance can be achieved with the doped MnO_2 cathode. The undoped and doped cathodes retain more than 80% and 75% of their initial capacity, respectively, over 10 cycles. The good cycling and discharge characteristics achieved with the doped MnO_2 motivated to further characterize its product of the discharged and charged material.

2. Characterization of the Bi_2O_3-doped MnO_2 cathode material

With an objective to understand the influence of Bi_2O_3 in MnO_2 during the electrochemical processes, the discharged and charged cathode was subjected to SIMS, XRD, FTIR, and TEM characterization.

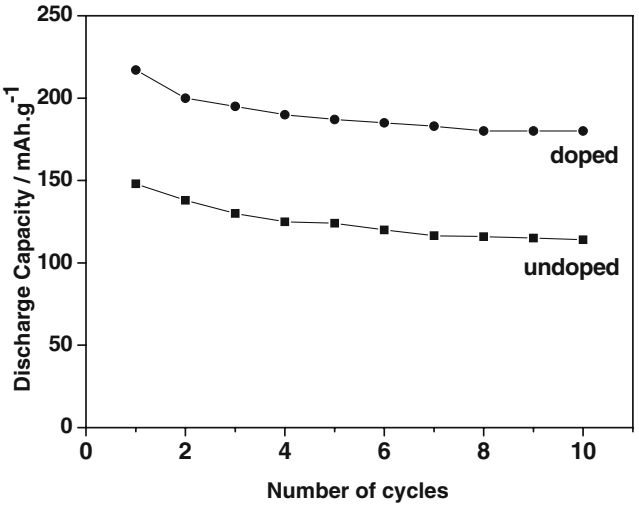

Fig. 2 Variation of discharge capacity as a function of cycle number for undoped and Bi_2O_3-doped MnO_2 cathode

In order to understand the discharge mechanism, the undoped and doped MnO_2 were subjected to SIMS depth profile analysis. The Li^+ ions insertion into the MnO_2 structure is confirmed from the SIMS analysis. The Fig. 3a, b shows the depth profile analysis in the Li^+ ion counts as obtained by SIMS technique of the undoped and Bi_2O_3-doped MnO_2 after its first discharge. The data show that 25 μm below the surface of the discharged MnO_2 (in the bulk), the Li^+ ion concentration is present. However, the concentration of lithium ions in the Bi_2O_3-doped cathode is higher than that undoped MnO_2 material. This explains the difference in discharge capacity observed for doped material in Fig. 1 and, hence, its improved rechargeability.

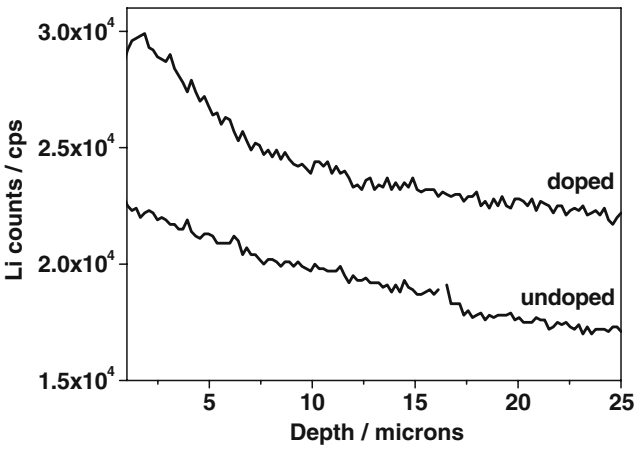

Fig. 3 SIMS depth profile analysis for lithium species on the (a) *undoped* and (b) Bi_2O_3-*doped* MnO_2 cathode. It shows consistently a higher amount of Li^+ ions in the Bi_2O_3-doped MnO_2

The discharged and charged products of doped MnO_2 cathodes have been investigated by X-ray diffraction. An analysis of the XRD data (Fig. 4a) of the Bi_2O_3-doped MnO_2 before discharge shows a characteristic peaks of MnO_2 (+) (JCPDS card 24-0735) in addition to peaks corresponding to Bi_2O_3 (B) and a main Bragg reflection corresponding to graphite (acetylene black) at $2\theta=26°$ (C). A noticeable change occurs in the XRD pattern after 50% discharge (Fig. 4b) referred to as "mid-discharge." The new reflections with sharp peaks (filled circle) and a few shoulder peaks (empty circle, asterisk, empty square) are seen in Fig. 4b. As indexed in the XRD pattern (Fig. 4b), these reflections were in good agreement with those reported for the mineral of formula Li_xMnO_2, i.e., lithium-intercalated MnO_2 (JCPDS cards 44-0143, 35-0749, and 44-0147). This could be interpreted as lithium ions from the electrolyte having been inserted into the host MnO_2 [12]. Minor reflections are identified as Mn_2O_3 (asterisk), MnO (empty square), and MnOOH (empty circle) in the mid discharged cathode. These secondary compounds are reported to be commonly formed when aqueous based Zn/MnO_2 cells are discharged [18]. It is well known that these compounds are electrochemically inactive. During this "mid-discharge" reduction process, the cell voltage decreases continuously from 1.7 to 1.45 V as seen in Fig. 1. On further discharge to 100% (referred to as "full discharged"), the reflections (Fig. 4c) corresponding to lithium-intercalated manganese oxide (filled circle) peaks becomes sharper while the peaks corresponding to MnOOH (empty circle) disappears. During the long discharge process, lithium ions are further intercalated so that the Mn^{4+} ions are further reduced to Mn^{3+}. This process corresponds to the potential region (1.4–1.2 V) as seen in Fig. 1. During this process, the Bi^{3+} acts as a pillar in the interlayer spacing of MnO_2 structure and preventing the formation of spinel lattice and dissolution of Mn^{3+} ions from the solid MnO_2 [16]. This result reveals that Bi_2O_3 doping are effective in suppressing the formation of unwanted discharge products such as birnessite (δ-MnO_2) and hausmannite (Mn_3O_4) and γ-Mn_2O_3 spinel lattices [18, 19] while forming lithium intercalated MnO_2. This is also evident from FTIR spectra shown in Fig. 5. Figure 4d also shows the XRD pattern of the cathode material after recharging the fully discharged battery. A decrease in intensity of the peaks corresponding to Li_xMnO_2 (filled circle) occurs. Hence, we infer that the lithium intercalation process is electrochemically reversible.

The FTIR spectra of doped MnO_2 materials are shown in Fig. 5. The material before discharged had three peaks labeled A, B, and C. The peaks below the region of 800 cm^{-1} (Fig. 5) are assigned to fundamental vibrations of MnO_6 octahedra. The peaks "B" and "C" at 1,200 and 875 cm^{-1} are the fundamental O–H bending mode [20, 21] and C–O bond in Li_2CO_3 [22]. A noticeable thing in the spectra (Fig. 5c) is that on long discharge, additional peaks A_1 and B_1 are seen. The peak at A_1 could suggest the formation of lithium intercalated MnO_2 in which the Mn is in the Mn (III) oxidation state. The peak at B_1 is due to the formation of manganese oxide species. The spectra obtained for the charged material (Fig. 5d) shows that the process is reversible. The results obtained from the XRD

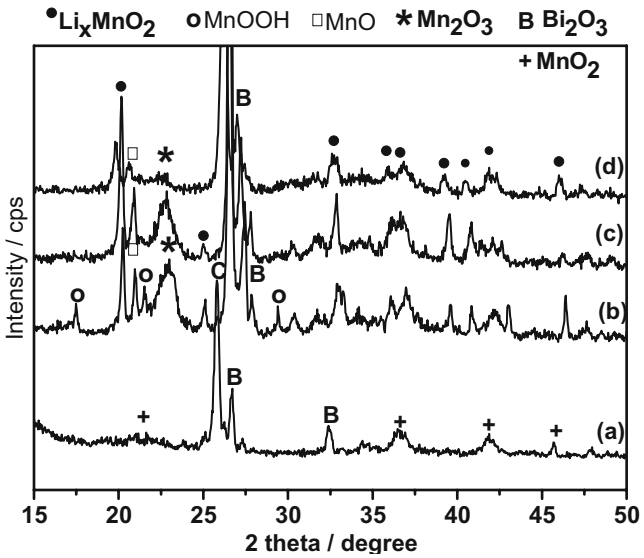

Fig. 4 XRD pattern of MnO_2 mixed with Bi_2O_3 and AB (Acetylene black) and PVDF (binder) *a* before discharged, *b* mid-discharged, *c* full discharged, and *d* charged after discharge in LiOH electrolyte

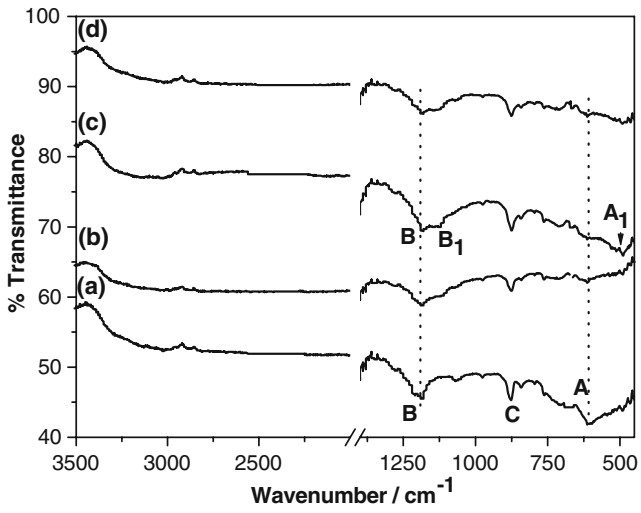

Fig. 5 Infrared spectra of Bi_2O_3-doped MnO_2 cathode *a* before discharge *b* mid-discharged *c* full discharged, and *d* charged after discharge in LiOH electrolyte

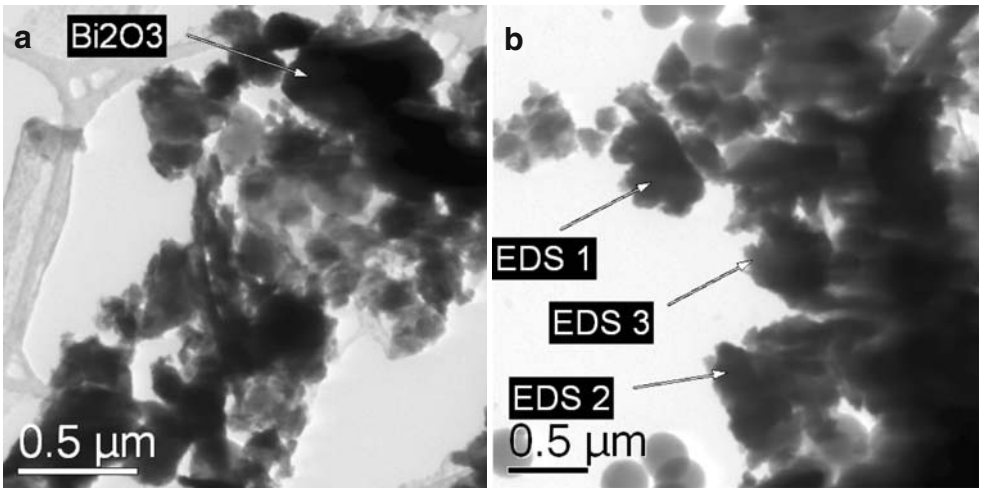

Fig. 6 TEM images of Bi_2O_3-doped MnO_2 cathodes **a** before and **b** after discharge

and FTIR spectroscopy confirms that stabilizing effect of the Bi^{3+} ions in the MnO_2 structure enhances the lithium insertion-extraction mechanism.

In order to gain insight into the distribution of Bi_2O_3 on MnO_2 cathode and its role on discharge mechanism, we have used TEM and SIMS analysis to study this. Figure 6a, b shows TEM images of doped MnO_2 before and after discharge. From Fig. 6a, it can be seen that Bi_2O_3 particles form like a cluster on the MnO_2 cathode. For the same material after discharge (Fig. 6b), no presence of Bi_2O_3 particles is observed through EDS; otherwise, it could be unevenly distributed in the cathode. This suggests that while discharging, Bi-containing particles are in intimate contact with manganese [23, 24]. Figure 7 represents the depth profile results for a bismuth species of the Bi_2O_3-doped MnO_2 cathode. It can be seen that the counts for bismuth is low for the discharged cathode. These results indicate that bismuth involved in the electrochemical process and thus renders a good rechargeability. However, the exact mechanism of bismuth participation needs to be established.

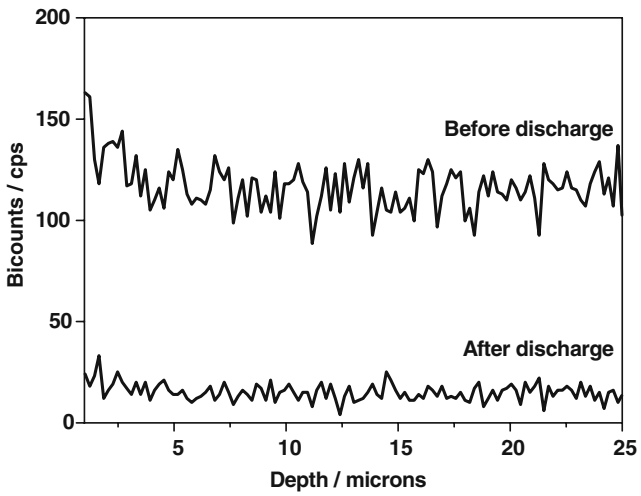

Fig. 7 SIMS depth profile analysis for bismuth species on the Bi_2O_3 doped MnO_2 cathode (a) *before* and (b) *after discharge*. It shows relatively a lower amount of Bi ions in the after discharged cathode

Conclusions

The discharge–charge behavior of a Bi_2O_3 doped MnO_2 in a zinc alkaline battery containing aqueous LiOH battery has been investigated. The doped MnO_2 cathode with an electrolyte selection pH=10.5 has been shown to exhibit a discharge capacity of 215 mAh/g as compared to 150 mAh/g with pH=12.0 (reported in ref. 12) using a 1-V cutoff voltage for both the cells. The doped cathode retains more than 80% of its initial capacity after 10 cycles. With optimum electrolyte selection, better cycling performance is seen. The SIMS depth profile analysis showed that the lithium insertion mechanism is involved during discharge process. The X-ray diffraction and the infrared spectroscopy results confirm that the presence of Bi_2O_3 enhances the lithium intercalation mechanism while preventing the formation of nonrechargeable products. The energy dispersive analysis associated with transmission electron microscopy and SIMS techniques showed that Bi_2O_3 is involved while discharge although the exact participation is unclear. The doped MnO_2 material with appropriate pH selection has been proved to given higher electrochemical performance a suitable cathode for a secondary battery.

Acknowledgements The author would like to thank the Australian Nuclear Science and Engineering for providing financial assistance (AINGRA award 08048) to enable work on SIMS facilities at Australian Nuclear Science and Technology Organization.

References

1. Fritsch S, Navrotsky A (1996) J Am Ceram Soc 79:1761, doi:10.1111/j.1151-2916.1996.tb07993.x
2. MacNeil DD, Lu Z, Chen Z, Dahn JR (2002) J Power Sources 108:8, doi:10.1016/S0378-7753(01)01013-8
3. Greenwood NN, Earnshaw A (1984) Chemistry of the Elements, 1st edn. Pergamon, Oxford
4. Boden D, Venuto CJ, Wisler D, Wylie RB (1968) J Electrochem Soc 115:333, doi:10.1149/1.2411182
5. Sajdl B, Micka K, Krtil P (1995) Electrochim Acta 40:2005, doi:10.1016/0013-4686(94)E0163-T
6. McBreen J (1975) Electrochim Acta 20:221, doi:10.1016/0013-4686(75)85028-6
7. Im D, Manthiram A, Coffey B (2003) J Electrochem Soc 150:1651, doi:10.1149/1.1622960
8. Kordesch K, Weissenbacher M (1994) J Power Sources 51:61, doi:10.1016/0378-7753(94)01955-X
9. Mondolini C, Laborde M, Rioux J, Andoni E, Levy-clement C (1992) J Electrochem Soc 139:954, doi:10.1149/1.2069374
10. Kozawa A, Powers RA (1996) J Electrochem Soc 113:870, doi:10.1149/1.2424145
11. Minakshi M, Singh P, Issa TB, Thurgate S, DeMarco R (2004) J Power Sources 130:254, doi:10.1016/j.jpowsour.2003.12.018
12. Minakshi M, Mitchell DRG (2008) Electrochim Acta 53:6323, doi:10.1016/j.electacta.2008.04.013
13. Minakshi M, Singh P, Carter M, Prince K (2008) Electrochem Solid-State Lett 11:145, doi:10.1149/1.2932056
14. Bach S, Ramos JPP, Baffier N, Messina R (1995) Electrochim Acta 40:785, doi:10.1016/0013-4686(94)E0170-5
15. Ghavami RK, Rafiei Z, Tabatabaei SM (2007) J Power Sources 164:934, doi:10.1016/j.jpowsour.2006.10.084
16. Wroblowa HS, Gupta N (1987) J Electroanal Chem 238:93, doi:10.1016/0022-0728(87)85167-7
17. Gao YF, Gupta N, Wroblowa HS (1987) J Electroanal Chem 238:107
18. Kordesch K, Gsellmann J, Peri M, Tomantschger K, Chemelli R (1981) Electrochim Acta 26:1495, doi:10.1016/0013-4686(81)90021-9
19. Raghuveer V, Manthiram A (2005) Electrochem Commun 7:1329, doi:10.1016/j.elecom.2005.09.012
20. Novak A (1974) Struct Bonding, Berlin 18:177–216
21. Wu YT, Hu CC (2005) Electrochem Solid-State Lett 8:A240, doi:10.1149/1.1874673
22. Aurbach D, Daroux ML, Faguy PW, Yeager E (1987) J Electrochem Soc 134:1611, doi:10.1149/1.2100722
23. Qu D, Diehl D, Conway BE, Pell WG, Qian SY (2005) J Appl Electrochem 35:1111, doi:10.1007/s10800-005-9005-y
24. Kannan AM, Bhavaraju S, Prado F, Manivel Raja M, Manthiram A (2002) J Electrochem Soc 149:483, doi:10.1149/1.1459713